Impact-induced bonding and boundary amorphization of TiN ceramic particles during room temperature vacuum cold spray deposition

Yi Liu[a,*], Yuyue Wang[b], Xinkun Suo[a], Yongfeng Gong[a], Chang-jiu Li[b], Hua Li[a,*]

[a]Key Laboratory of Marine Materials and Related Technologies, Zhejiang Key Laboratory of Marine Materials and Protective Technologies, Ningbo Institute of Materials Technology and Engineering, Chinese Academy of Sciences, Ningbo 315201, China
[b]State Key Laboratory for Mechanical Behavior of Materials, Xi'an Jiaotong University, Shaanxi 710049, China

Abstract

Vacuum cold spray (VCS) has been developed as a competent technique for room temperature bulk coating fabrication of solid ceramic particles. Here we report formation and densification mechanisms of VCS TiN ceramic coatings as elucidated by characterizing their microstructures at particle/substrate and particle/particle interfaces. TEM observation reveals apparent fracturing and plastic deformation of TiN particles during impact deposition. The deformation located at the interfacial areas exhibits a dislocation density of $\sim 5 \times 10^{17}/m^2$. Formation of an amorphous layer with the width of 3–4 nm at the fringes of the ceramic particles is revealed. Impact velocity and high strain rate of TiN particles as determined by numerical computation further indicates the substantial role of the impact-induced plastic deformation in regulating the fabrication of the coatings. The results shed light on efficient room temperature bulk fabrication of ceramic materials with tunable structures.
© 2015 Elsevier Ltd and Techna Group S.r.l. All rights reserved.

1. Introduction

As one of the most recently developed coating techniques, cold spray offers competitive advantages and exciting opportunities for heat-sensitive materials for bulk coating fabrication [1]. Adhesive strength of the coatings is one of the crucial variables that affect their long-term service performances. It is well established that the bonding mechanism of thermal sprayed coatings lies primarily in mechanical interlocking [2,3]. Bonding strength could be further enhanced via splat-holding, metallurgical/diffusion bonding, or other chemical bonds by virtue of pre-/post-spray treatment [3,4]. Cold spray provides sprayed particles with strong intrinsic mechanical interlocking and metallurgical bonding could be further gained for enhanced adhesion [5]. During cold spray deposition, bonding of the particles prevails only when their impact velocities exceed a critical value. This critical velocity depends not only on chemistry of the powder materials, but also on powder quality, particle size and particle impact temperature [6]. Clarification of bonding mechanisms of the powder particles during cold spray is of essential importance towards extensive applications of the promising coating technique.

Certain research efforts made in recent years proposed thermal softening as the main regime of the interaction between cold sprayed particles at the site of impact and particle deforms with a very high strain rate [7,8]. Solid state cold-welding was realized responsible for the bonding of sprayed particles with substrate during cold spray, which might be attributed to plastic deformation with high strain rate associated with adiabatic shear instabilities at particle/substrate interfaces [7–9]. However, it should be noted that the above mentioned bonding mechanisms mostly apply to metals or metal-matrix composites, knowledge on cold sprayed ceramic coatings needs to be further explored. As an alternative coating technique, vacuum cold spray (VCS) is a recently developed room-temperature deposition approach based on shock-loading solidification [10–14]. VCS is of particular prospect for its outstanding advantages of fabricating ceramic coatings with high deposition

*Corresponding authors. Tel.: +86 574 86686224; fax: +86 574 86685159.
E-mail addresses: liuyi@nimte.ac.cn (Y. Liu), lihua@nimte.ac.cn (H. Li).

efficiency ranging from several to tens of microns per minute. Yet, unfortunately, fundamental understanding of VCS falls far behind its practical applications, partly due to the difficulties in clafifying the bonding mechanisms of ceramic particles during coating deposition. It was proposed that during the VCS impact consolidation, upon the impingement of sprayed particle onto substrate, part of particle's kinetic energy is converted into thermal energy, causing increase in temperature at impact point [11]. Heat and high pressure might in turn promote bonding at substrate-particle interface and between multiple particles as well [11,15]. However, how exactly the bonding takes place remains enigmatic and a conclusive answer to this question might need detailed microstructural information of the coatings at critical locations.

In spite of the impact bonding speculations, there exist some exciting phenomena in VCS ceramic coatings and adequate bonding of ceramic particles with substrate or among themselves at room temperature needs to be elucidated. As a typical ceramic material, titanium nitride (TiN) is a transition metal nitride with covalent, metallic and ionic bonding and exhibits certain metal properties [16]. In this paper, we report impact velocity and high strain rate of TiN particles during VCS deposition and high resolution microstructure of the coatings, revealing the bonding mechanisms of TiN coatings that may be applicable to other ceramic materials during VCS bulk coating fabrication.

2. Materials and methods

Commercially available TiN powder (Mok Advanced Material Technology Co. Ltd., China) with an average size (D_{50}) of 1.6 μm was used for coating deposition. The particle size was measured by using a laser particle size analyzer (Mastersizer 2000, Malvern, UK). To clarify the impact behaviors of the particles at particle/substrate interface, polished silicon wafers with the thickness of 200 μm were used as the substrates for the coating deposition. Prior to the spraying, the wafers were cleaned by sonication in acetone bath and the powder was dried overnight at 120 °C. The VCS-2000 VCS system developed by Xi'an Jiaotong University, China was used to deposit the coatings. Detailed operation procedures of the system were described previously [12]. Helium gas with the flow rate of 7.5 l/min was used for feeding and accelerating the powder particles. The scanning speed of 15 mm/s and the spray distance of 10 mm were adopted for the coating deposition. During the VCS processing, the substrate temperature never exceeded 30 °C. The laser Doppler anemometry and PVT-MS1 system (developed by Xi'an Jiaotong University, China) were employed to measure the particle velocity.

Microstructure of the powder and the coating samples was characterized by transmission electron microscopy (TEM, JEM-3010, Japan) and field emission scanning electron microscopy (TESCAN-VEGA XMU, Czech Republic). High resolution transmission electron microscopy (HRTEM) was employed for characterizing the structural evolution of the interfacial areas between coating and substrate and among individual impacted particles at near-atomic-scale. Phase composition of the samples was detected by X-ray diffraction (XRD, Rigaku-D/max2400, Japan) with CuKα ($\lambda = 1.5405$ Å) radiation operated at 40 kV and

100 mA. The goniometer was set at a scan rate of 2°/min over a 2θ range of 30–80 °.

To examine the impact behaviors of the TiN particles during VCS spraying, numerical simulations were performed using the commercial software ANSYS-FLUENT 14.5 to predict gas flow and particle velocity. Self-developed nozzle had the configuration dimensions of particle (gas) inlet diameter of 4 mm, convergent length of 40 mm, throat diameter of 0.44 mm, divergent length of 30 mm, and outlet diameter of 3.5 mm. The sizes exactly matched the real VCS gun used in this study. Two-dimensional axis-symmetric model was employed for saving computation time. Sketch of the computational domain, corresponding boundary conditions and selected local grids are shown in Fig. 1. The computational domain was meshed into 494,600 quadrilateral cells for achieving a grid-independent solution. The grids at some key regions were refined to guarantee computational accuracy. Velocity of the particles was computed using the discrete phase modeling. The stochastic-tracking model was used to subsume the turbulence-induced particle dispersion. In this approach, the discrete random walk model was used to predict the particle velocity. A MATLAB code (MathWorks Inc.) was developed to calculate the mean particle velocity.

3. Results and discussion

3.1. Microstructure and phases of the coatings

The starting TiN particles exhibit irregular contours (Fig. 2a). Dense TiN coating with the thickness of ~20 μm was successfully fabricated on silicon wafer (Fig. 2b-1). It was realized that the deposition rate for TiN coatings can be tailored ranging from 5 to 30 μm/min for a coating area of 900 mm^2. The grain refinement with randomly oriented nanosized grains in the coating is clearly seen (Fig. 2b-1 and b-2). The initial TiN particles have the size of ~500–2000 nm (Fig. 2a). In contrast, however, the maximum size of the TiN particles in the as-deposited coating dropped to ~200 nm (Fig. 2b), evidencing significantly reduced grain size for the particles after the VSC processing.

Since the coating fabrication was made in vacuum environment, it is not surprising that the chemistry of the starting TiN was completely retained in the as-deposited coatings (Fig. 2b). In fact, the particles are deposited in solid state to form the coatings at room temperature. However, broadened XRD peak is seen for the coating as compared to that for the starting powder (Fig. 2c), which is presumably attributed to grain refining and microstrain broadening in the coatings.

Numerical analysis by Chun et al. already suggested that bonding of ceramics involves fragmentation of submicron-sized ceramic particles into nanoparticles and successive impact exerted by other particles, which provides sufficient bonding energy to nanoparticles fragmented by shock wave [15]. Fragmentation of TiN particles predominately takes place during coating formation stage. In addition, HRTEM characterization of the coatings clearly shows multiplication of dislocations at particles' boundary regions (Fig. 3). The domains located relatively far away from the boundaries exhibit defect-free crystal fringes, whereas defect-like
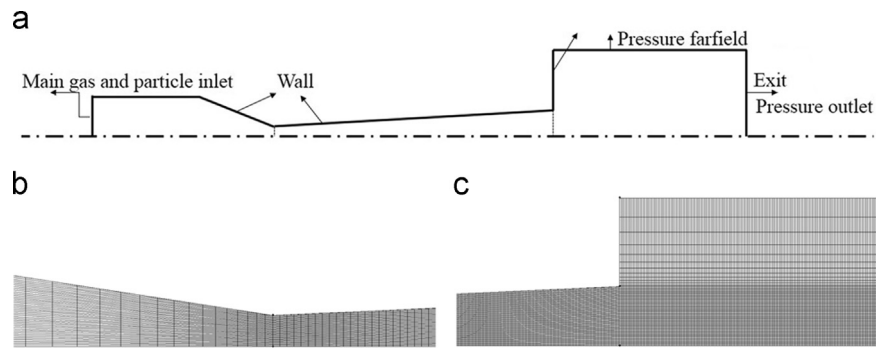
Fig. 1. Diagrammatic sketch of the numerical simulation model (a), the local grid in the divergent section (b) and jet region (c).
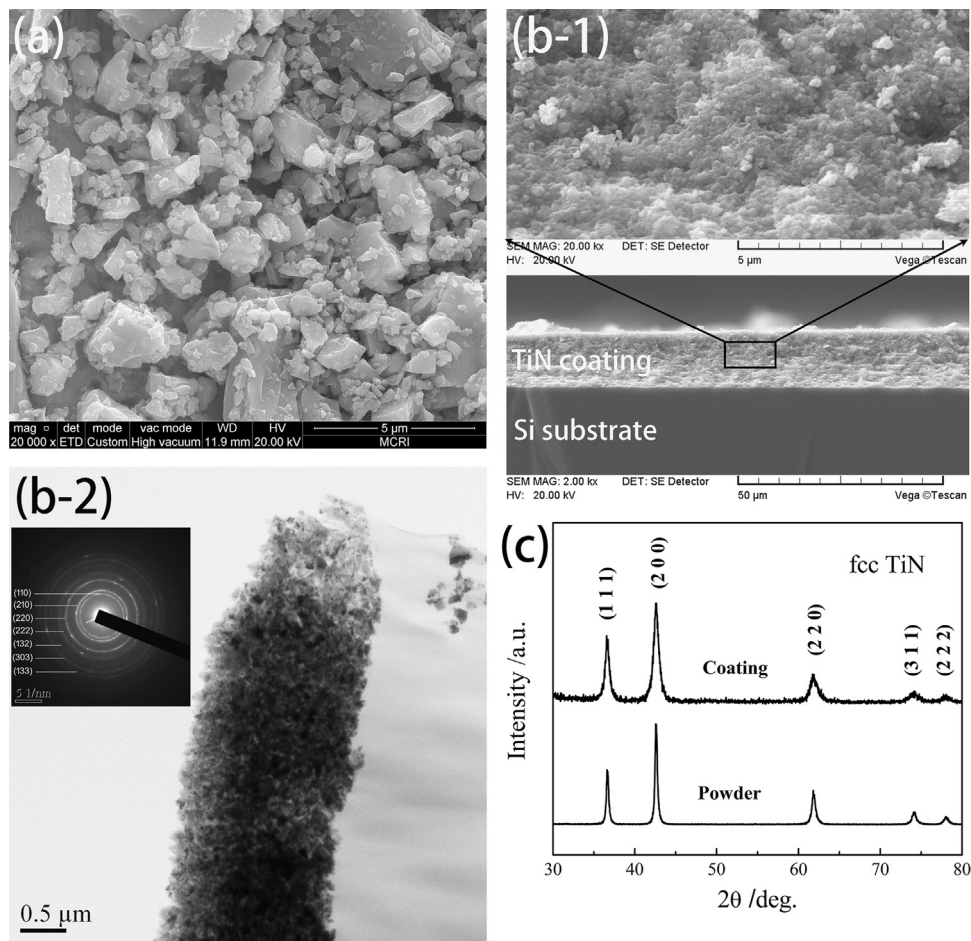

Fig. 2. Characteristics of the starting TiN powder and the VCS coatings, (a) FESEM image of the starting TiN powder, (b) cross-sectional images of the TiN coatings, and (c) the XRD spectra of the starting powder and the coatings (The inset in b-2 is SAED pattern of the coatings evidencing the sole presence of TiN).

dislocations are displayed within the boundary regions. This indicates the predominate effect of impact-induced deformation on the formation of the dislocations. The motion of dislocations usually triggers plastic deformation. When materials are plastically deformed, certain fraction (roughly 5%) of energy is retained internally, and the remainder is dissipated as heat [17]. This stored strain energy correlates closely to dislocations. In this case, a high density dislocation with dislocation density of up to $5 \times 10^{17}/m^2$ is revealed after individual particle impact. It is noted that the density of the dislocations realized in the starting TiN particles at their fringes is $\sim 7 \times 10^{16}/m^2$ (HRTEM image not shown). Therefore, the dislocations exhibited by the coating should be mainly attributed to particle impact during coating formation stage. Lattice distortions existing around the dislocation line are responsible for lattice microstrain [18,19]. It was speculated that high defect density coupled with energy fluctuation could activate diffusion process [20,21]. For the VCS TiN
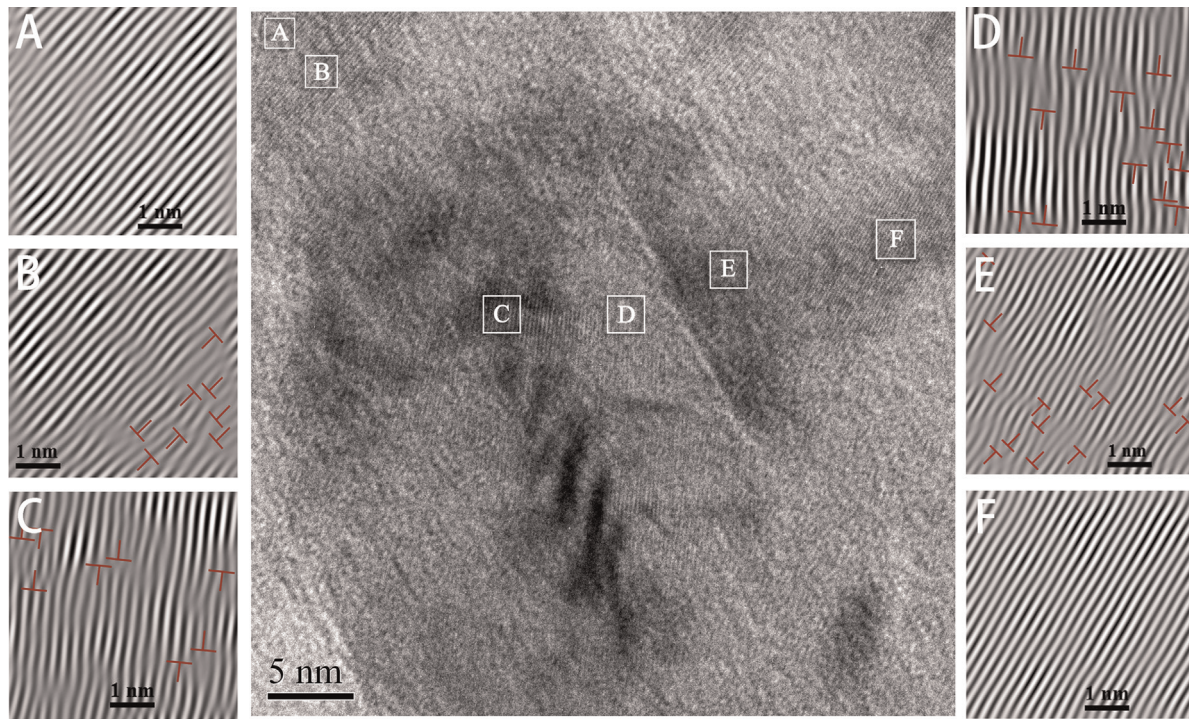
Fig. 3. HRTEM image of the TiN coating and inverse FFT filtered pictures derived from the image. High density of dislocations located at the areas close to particles' interfaces is suggested.

coatings, likely enhanced diffusion should promote bonding of individual solid particles during the coating formation.

3.2. Impact behaviors of the TiN particles

Numerical simulation reveals impact characteristics of individual TiN particles during the VCS deposition (Fig. 4a). The impact velocity varies from 300 to 1100 m/s depending on the size of the particles as determined by finite-element method (FEM) analyses. Measurement by laser Doppler anemometry and PVT-MS1 showed that the velocity of in-flight particles during the spraying is 200–800 m/s. The values are in good agreement with the simulated results, taking into account that the size of majority of the TiN particles used in this study is ~1.6 μm (the inset in Fig. 4a). It has been pointed out that the maximum local temperature rise of lower than 773 K and the shock pressure of 2.5 GPa at the impact point are insufficient for ceramic sintering [22]. As a typical ceramic material, TiN does not have the dislocation mobility as metals do due to its distinctive atomic bond type and limited slip system. During the coating formation stage, the temperature attained by the particles is not sufficient to accomplish melting, one of the possibilities to release the kinetic energy of the consecutive particle-on-particle and particle-on-substrate collisions is to fracture or deform plastically. Most of the impact energy might be used for creating new fracture surfaces. In fact, microcracks within TiN particles in the as-sprayed coatings are clearly seen (Fig. 4b), suggesting the tendency of the particles towards fracturing during high velocity/pressure shock loading. The

fracturing of individual TiN particles is schematically shown in Fig. 4c.

It has been recognized that during cold spray deposition of metal particles, in order to build up a deposit successively, plastic deformation is essentially required for both particles and substrate upon the impact of high velocity solid particles [9]. Upon impinging on solid substrate, metallic particles can stick to or penetrate into the substrate depending on the critical deposition velocity [23], which crucially decides if rebounding or erosion phenomena would occur. For the VCS TiN coating, presumable erosion of the silicon wafer substrate at its surface is clearly seen (Fig. 5). As particles penetrate the substrate, craters are developed at substrate surface. TiN particles are embedded into the substrate, which might in turn promote adhesion of the coating. High degree deformation around the contact boundary is enhanced by adiabatic shear instability, usually leading to formation of jetting [24]. Compared to metals, the ceramic particles possess very limited deformability. The jets of individual TiN particles in the first layer of the coating are realized (Fig. 5). The jetting and impact accumulation of individual TiN particles is also depicted (the inset in Fig. 5). Interfacial jet is able to remove adsorbed contamination film from the surfaces of both particles and substrate, enabling an intimate contact of clean surfaces and hence promoting particle/substrate bonding. Similar results have also been reported that during vacuum kinetic spraying, plastic deformation was generated in alumina particles as a result of shock loading, and impact intensity of the particles remarkably affect their fragmentation behavior and consolidation of previously deposited layer [25].
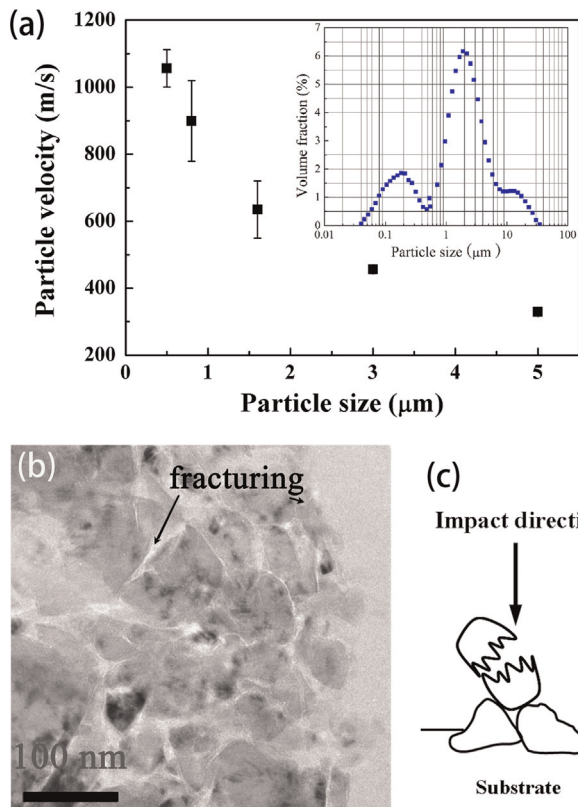
Fig. 4. (a) Impact velocity as a function of particle size for the TiN particles during the VCS processing. The inset image shows the particle size distribution of the starting TiN feedstock powder used in this study. (b) Bright field cross-sectional TEM image of the TiN coating showing accumulation of individual solid state TiN particles and the microcracks within individual particles generated during coating formation stage. The fracturing of TiN particles during the VCS deposition as a consequence of releasing in part the impact energy is schematically shown in (c).
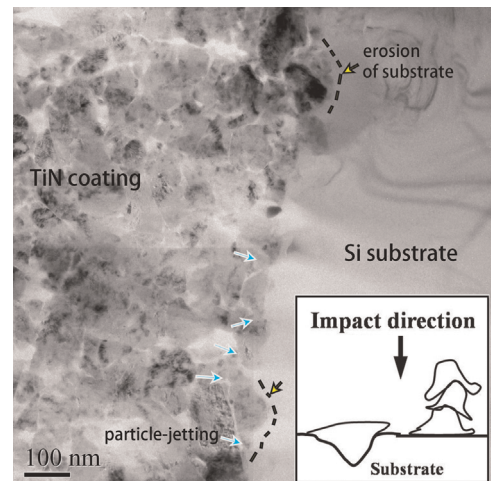

Fig. 5. Cross-sectional TEM image of the TiN coating showing the morphology of coating-substrate interfacial area, deformation and jetting of individual particles. Some particles are embedded into the substrate and induced erosion of the substrate. The inset is the schematic depiction of deformation and jetting of individual TiN particles during the VCS deposition.

Plastic deformation can be characterized by strain. The strain rate, ν, is correlated to stress impact pressure σ and strain ε by the following equation [26]: $\nu = \frac{\varepsilon}{t}$, where $\varepsilon = \frac{\sigma}{E}$ and $\sigma = \frac{V_0}{2}\sqrt{E\rho}$, E and ρ are Young's modulus ($\sim$251 GPa) and density ($\sim$5.44 g/cm^3) of TiN, respectively, and V_0 is particle velocity at the collision. In this study, as the particle impact velocity is 200–1100 m/s, the calculated impact pressure, σ, is 3.70–20.35 GPa. In this case, the particles undergo only limited deformation with a strain of 0.015–0.081 within 0.01–1.6 ns [15]. The corresponding strain rate during the kinetic spray impact is 1.0×10^7–8.1×10^9 s^{-1}. The maximum impact pressure attained at the contact interfaces supplies sufficient energy to trigger the strain, which further leads to generation of microcracks within (Fig. 4) and fragmentation of (Fig. 5) the ceramic particles. For cold spray processing, FEM analysis already suggested that strain rate of the impact zone by a metallic particle with the velocity of 680 m/s can reach 10^9 s^{-1} [5] and the impact pressure can reach up to 30 GPa [27]. For the VCS TiN coatings investigated in this research, both the strain rate and the impact pressure are relatively low, likely due to the vacuum processing environment and the physiochemical features of the ceramic material.

3.3. Interfacial structures

Cold welding regulates the bonding state of most sprayed materials depending on their initial contact area and diffusion rate [28]. The materials would not bond with each other if one of them is not malleable or contains surfaces with relatively thick oxygen layer or thin contaminant film. Likewise, if the two bonded parts are exposed to an oxygen-rich environment or certain other reactive compounds, cold welding would not be possible [29]. VCS technique intrinsically avoids the aforementioned limitations, providing the conditions required for the promulgation of solid-state reactions at low temperature through relieving the effect of product barriers on reaction kinetics. It is therefore unsurprising to note that TiN particles have been cold-welded and consolidated at room temperature during the VCS processing (Fig. 6a). The high density of grain boundaries and better inter-particle contact under the high impact pressure of 3.70~20.35 GPa likely result in high diffusion rate. In addition, multiple collisions bring about fragments and consequently increased fresh fractured surfaces for activated diffusion processes, which in turn facilitates the cold-welding. Similar deformation and cold welding of individual TiN particles in ball-milled TiN coating have also been observed by other research groups [30,31].

In addition to the plastic deformation and cold-welding phenomena taking place at both the particles' interfaces and particle/substrate interface, formation of an amorphous layer was revealed at the places in between adjacent particles (Fig. 6b). HRTEM examination of the coating already shown in Fig. 3 also discloses different crystallographic orientations at different particles' interfaces, which are suggested by the (311), (220) and (200) planes of TiN. The image shows the interfaces for three individual TiN particles. Fast fourier transforms (FFTs) patterns taken from the three particles (box 1, box 3 and box 5 in the image) show a reciprocal
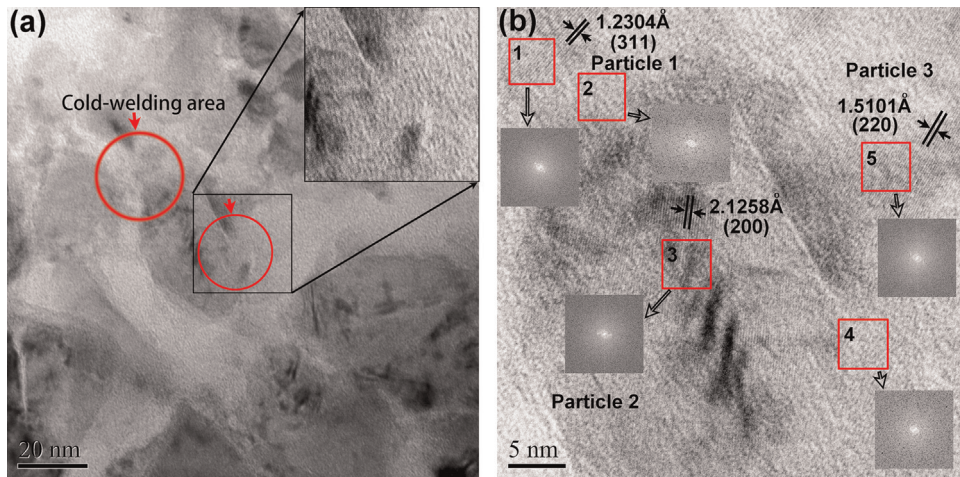
Fig. 6. TEM images of the VCS TiN coating, (a) the image acquired from cross-section of the coating show clearly cold welding zones, and the zones are typically surrounded by the circles and the inset shows enlarged view of the selected area, and (b) typical HRTEM image of the TiN coating shows presence of an amorphous layer located at the particles' boundaries. The boxes 1, 3, and 5 highlight typical areas from three individual TiN particles. The boundaries between either of the three TiN particles are typically selected as surrounded by black boxes 2 and 4 for analyses. The inset FFT patterns of the selected box regions show diffuse haloes, which is a typical character of amorphous phase.

lattice indicative of the face-centered cubic (fcc) crystal structure of TiN. By comparison, FFTs taken from the interfacial areas (box 2 and box 4) exhibit diffuse haloes, which are typical character of amorphous phase. A bonding zone with a thickness of ∼3–4 nm at particles' interface is suggested. Taking into account the cold-welding at particles' interfaces, i.e. the area encircled by box 4 in the image, an amorphous zone with an area > 25 nm^2 has already been resulted from the impact-induced bonding.

Strain-induced amorphization of materials is affected by several key factors, for instance adiabatic heating and rapid cooling at impact areas, deformability and glass forming ability of the materials [32]. Simulation results already suggested that the temperature attained by ceramic particles during VCS processing is below 600 K [15] or 773 K [21], much lower than the melting point of TiN, 3203 K. Therefore, formation of the amorphous layer is not caused by rapid cooling, instead it is likely a result of the shock impact of the particles. Molecular dynamic simulations suggested that the critical strain rate of $\sim 5 \times 10^{10}$/s–7×10^{10}/s is necessary for strain-induced amorphization for kinetic sprayed metallic particles [33,34]. Our results show that transition from crystalline to amorphous phase of submicron- or nano- sized ceramic particles sprayed at room temperature in vacuum could have already been activated with a strain rate of up to 10^9/s and a pressure of 3.70–20.35 GPa. It should be noted that TiN particles showed constrained deformation with the strain of 0.015–0.081. It is not unanticipated that the transition from amorphization to recrystallization observed in cold sprayed metallic coatings was not observed in the VCS TiN coating. It can thus be concluded that the localized shock amorphization occurs in ceramic particles as a direct result of the high pressure and high velocity collisions.

Based on the microstructural features of the VCS TiN coatings, a schematic depiction is proposed to illustrate the boundary
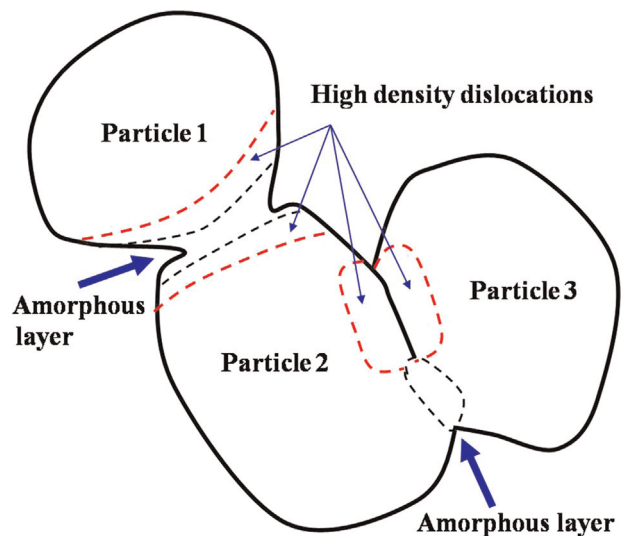

Fig. 7. Schematic illustration showing impact-induced high density dislocations and formation of amorphous layer at the ceramic particles' boundaries during the VCS coating deposition.

characteristics of TiN particles during VCS deposition (Fig. 7). The strain is easily resulted from high density dislocations upon high speed impact of individual particles. Amorphization of the ceramic particles at their fringes may be triggered by the development of large anisotropic elastic strains during impacting and subsequent violation of the Born stability conditions [35,36]. Those phenomena would result in crystal collapse along specific crystallographic orientations, in turn triggering the amorphization related to high pressure and high strain rate [33–37]. Directionally deformed initial grains with high dislocation density are next to the amorphous zone, indicating that the generation of dislocations during plastic deformation occurs at much lower stress than the

transition. The impact-associated phenomena facilitate the bulk coating fabrication of the ceramic material.

4. Conclusions

During vacuum cold spray processing, submiron-sized TiN particles experienced fracturing, plastic deformation with a strain rate of 1.0×10^7–$8.1 \times 10^9 \, s^{-1}$, and high strain rate-induced formation of amorphous structure at their fringes. The grain refinement, plastic deformation and cold welding of the ceramic particles provides the vacuum cold sprayed ceramics coatings with distinctive bonding regimes for both cohesion and adhesion. The particular features realized at the boundaries of as-deposited TiN particles such as presence of dislocations and localized amorphization give insight into exploring efficient ways to accomplish desired microstructures of ceramic coatings deposited by room temperature vacuum cold spray.

Acknowledgments

References

[1] K. Sakaki, Cold spray process: overview and application trends, Mater. Sci. Forum 449-452 (2004) 1305–1308.

[2] W.J. Trompetter, A. Markwitz, M. Hyland, P. Munroe, Evidence of mechanical interlocking of NiCr particles thermally sprayed onto Al substrates, J. Thermal Spray Technol. 14 (2005) 524–529.

[3] Y.Y. Wang, C.J. Li, A. Ohmori, Influence of substrate roughness on the bonding mechanisms of high velocity oxy-fuel sprayed coatings, Thin Solid Films 485 (2005) 141–147.

[4] L. Pawlowski, The Science and Engineering of Thermal Spray Coatings, 2nd ed., John Wiley & Sons, France, 2008.

[5] T. Hussain, D.G. McCartney, P.H. Shipway, D. Zhang, Bonding mechanisms in cold spraying: the contributions of metallurgical and mechanical components, J. Thermal Spray Technol. 18 (2009) 364–379.

[6] T. Schmidt, F. Gärtner, H. Assadi, H. Kreye, Development of a generalized parameter window for cold spray deposition, Acta Mater. 54 (2006) 729–742.

[7] H. Assadi, F. Gartner, T. Stoltenho, H. Kreye, Bonding mechanism in cold gas spraying, Acta Mater. 51 (2003) 4379–4394.

[8] M. Grujicic, J.R. Saylor, D.E. Beasleya, W.S. DeRosset, D. Helfritch, Computational analysis of the interfacial bonding between feed-powder particles and the substrate in the cold-gas dynamic-spray process, Appl. Surf. Sci. 219 (2003) 211–227.

[9] S. Yin, X. Wang, W.Y. Li, H. Jie, Effect of substrate hardness on the deformation behavior of subsequently incident particles in cold spraying, Appl. Surf. Sci. 257 (2011) 7560–7565.

[10] H. Kim, S.H. Cho, Y.J. Yoon, S. Yoo, Magneto-transport properties of $La_{0.7}Sr_{0.3}MnO_3$–manganese oxide composite films on YSZ substrates prepared using aerosol deposition, Ceram. Int. 41 (2015) 291–298.

[11] J. Akedo, Room temperature impact consolidation (RTIC) of fine ceramic powder by aerosol deposition method and applications to microdevices, J. Thermal Spray Technol. 17 (2008) 181–198.

[12] Y. Liu, Z.H. Dang, Y.Y. Wang, J. Huang, H. Li, Hydroxyapatite/graphene-nanosheet composite coatings deposited by vacuum cold spraying for biomedical applications: inherited nanostructures and enhanced properties, Carbon 67 (2014) 250–259.

[13] J.J. Park, D.Y. Kim, S.S. Latthe, J.G. Lee, M.T. Swihart, S.S. Yoon, Thermally induced superhydrophilicity in TiO_2 films prepared by supersonic aerosol deposition, ACS Appl. Mater. Interfaces 5 (2013) 6155–6160.

[14] S.G. Han, J. Ryu, W. Yoon, J. Choi, B. Hahn, J. Kim, D. Park, Effect of electrode and substrate on the fatigue behavior of PZT thick films fabricated by aerosol deposition, Ceram. Int. 38 (2012) S241–S244.

[15] D.M. Chun, S.H. Ahn, Deposition mechanism of dry sprayed ceramic particles at room temperature using a nano-particle deposition system, Acta Mater. 59 (2011) 2693–2703.

[16] T. Fu, X.H. Peng, Y.B. Zhao, R. Sun, S.Y. Weng, C. Feng, Z.C. Wang, Molecular dynamics simulation of TiN (001) thin films under indentation, Ceram. Int. 41 (2015) 14078–14086.

[17] N. Rebelo, S. Kobayashi, Handbook of refractory carbides and nitrides: properties, characteristics, processing, and applications, Int. J. Mech. Sci. 22 (1980) 699–705.

[18] C.J. Li, G.J. Yang, P.H. Gao, J. Ma, Y.Y. Wang, C.X. Li, Characterization of nanostructured WC-Co deposited by cold spraying, J. Thermal Spray Technol. 16 (2007) 1011–1020.

[19] P. Grahle, E. Arzt, Microstructural development in dispersion strengthened NiAl produced by mechanical alloying and secondary recrystallization, Acta Mater. 45 (1997) 201–211.

[20] J.E. Bailey, P.B. Hirsch, The dislocation distribution, flow stress, and stored energy in cold-worked polycrystalline silver, Philos. Mag. A 5 (1960) 485–497.

[21] L.C. Robert, Diffusion models for hot pressing with surface energy and pressure effects as driving forces, J. Appl. Phys. 41 (1970) 4798–4807.

[22] J. Akedo, Aerosol deposition of ceramic thick films at room temperature: densification mechanism of ceramic layers, J. Am. Ceram. Soc. 89 (2006) 1834–1839.

[23] D.L. Gilmore, R.C. Dykhuizen, R.A. Neiser, M.F. Smith, T.J. Roemer, Particle velocity and deposition efficiency in the cold spray process, J. Thermal Spray Technol. 8 (1999) 576–582.

[24] S.V. Klinkov, V.F. Kosarev, M. Rein, Cold spray deposition: significance of particle impact phenomena, Aerosp. Sci. Technol. 9 (2005) 582–591.

[25] H. Park, J. Kwon, I. Lee, C. Lee, Shock-induced plasticity and fragmentation phenomena during alumina deposition in the vacuum kinetic spraying process, Scr. Mater. 100 (2015) 44–47.

[26] J.A. Zukas, High Velocity Impact Dynamics, 1st ed., John Wiley & Sons, New York, 1990.

[27] J. Vlcek, L. Gimeno, H. Huber, E. Lugscheider, A systematic approach to material eligibility for the cold-spray process, J. Thermal Spray Technol. 14 (2005) 125–133.

[28] L. Lu, M.O. Lai, S. Zhang, Diffusion in mechanical alloying, J. Mater. Process. Technol. 67 (1997) 100–104.

[29] W. Zhang, N. Bay, Cold welding-theoretical modeling of the weld formation, Weld. J. 76 (1997) 417s–420s.

[30] S. Romankov, Y. Hayasaka, G. Kalikova, S.V. Komarov, N. Hayashi, E. Kasai, TEM study of TiN coatings fabricated by mechanical milling using vibration technique, Surf. Coat. Technol. 203 (2009) 1879–1884.

[31] S. Romankov, S.V. Komarov, E. Vdovichenko, Y. Hayasaka, N. Hayashi, S.D. Kaloshkin, E. Kasai, Fabrication of TiN coatings using mechanical milling techniques, Int. J. Refract. Mat. Hard Mater. 27 (2009) 492–497.

[32] Y.M. Xiong, K. Kang, G. Bae, S. Yoon, C.H. Lee, Dynamic amorphization and recrystallization of metals in kinetic spray process, Appl. Phys. Lett. 92 (2008) 194101–194103.

[33] H. Ikeda, Y. Qi, T. Cagin, K. Samwer, W.L. Johnson, W.A. Goddard, Strain rate induced amorphization in metallic nanowires, Phys. Rev. Lett. 82 (1999) 2900–2903.

[34] P.S. Branicio, J.P. Rino, Large deformation and amorphization of Ni nanowires under uniaxial strain: a molecular dynamics study, Phys. Rev. B 62 (2000) 16950–16955.

[35] J. Wang, S. Yip, S.R. Phillpot, D. Wolf, Crystal instabilities at finite strain, Phys. Rev. Lett. 71 (1993) 4182–4185.

[36] J.S. Tse, D.D. Klug, Mechanical instability of α-quartz: a molecular dynamics study, Phys. Rev. Lett. 67 (1991) 3559–3562.

[37] M.W. Chen, J.W. McCauley, K.J. Hemker, Shock-induced localized amorphization in boron carbide, Science 299 (2003) 1563–1566.